BIOCHEMISTRY
including biophysical chemistry & molecular biology

Article

pubs.acs.org/biochemistry

Structural Basis for the Inhibition of Human Lysozyme by PliC from *Brucella abortus*

Si-Hyeon Um,[†] Jin-Sik Kim,[†] Kuglae Kim,[‡] Nahee Kim,[‡] Hyun-Soo Cho,[‡] and Nam-Chul Ha*[,†]

[†]College of Pharmacy and Research Institute for Drug Development, Pusan National University, Busan 609-735, Republic of Korea
[‡]Department of Systems Biology, College of Life Science and Biotechnology, Yonsei University, Seoul, Republic of Korea

Supporting Information

ABSTRACT: Lysozymes are the first line of defense for a diverse range of organisms that catalyze the degradation of bacterial peptidoglycan. Gram-negative bacteria produce proteinaceous lysozyme inhibitors to protect themselves from the action of lysozymes. To date, MliC or PliC (membrane-bound or periplasmic inhibitor of c-type lysozyme, respectively) has been found in various Gram-negative bacteria. Here, we report the crystal structures of *Brucella abortus* PliC and its complex with human c-type lysozyme. The complex structure demonstrates that the invariant loop of MliC/PliC plays a crucial role in the inhibition of lysozyme via its insertion into the active site cleft of the lysozyme, as previously observed in the complex structure of *Pseudomonas aeruginosa* MliC and chicken c-type lysozyme. We identified a new binding interface between a loop adjacent to the active site of human lysozyme and a loop carrying Glu112 of *B. abortus* PliC, the structure of which was disordered in *P. aeruginosa* MliC. Because MliC/PliC family members have been implicated as putative colonization or virulence factors, the structures and mechanism of action of MliC/PliC will be relevant to the control of bacterial growth in animal hosts.

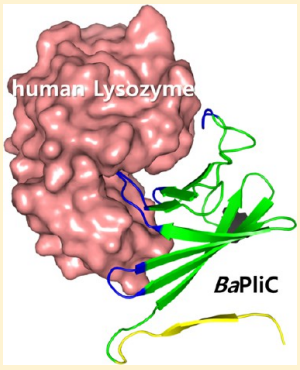

The innate immune system employs lysozymes as important components in a diverse range of organisms, including plants, invertebrates, and vertebrates. Lysozymes can degrade the bacterial cell wall by hydrolyzing the β-1,4-glycosidic bond between *N*-acetylmuramic acid and *N*-acetylglucosamine of peptidoglycan.[1−3] In vertebrates, lysozyme is found in tears, saliva, nasal secretions, the digestive tract, the respiratory airway, milk, and/or egg white. Lysozymes in the animal kingdom are classified as types c (chicken), g (goose), and i (invertebrate); only c-type lysozymes are found in humans.[4]

Because the peptidoglycan layer of Gram-negative bacteria is covered by the outer membrane, only a small portion of lysozyme can access the peptidoglycan layer. Thus, its activity is boosted when the permeability of the membrane is increased by the action of membrane-permeabilizing agents such as lactoferrin.[5−7] Highly specific proteinaceous inhibitors of lysozyme have been identified in diverse Gram-negative bacteria; these inhibitors are localized in the periplasmic space and confer lysozyme resistance to the bacteria.[7−10] Ivy (inhibitor of vertebrate lysozyme) and MliC/PliC (membrane-bound or periplasmic lysozyme inhibitor of c-type lysozyme, respectively) have also been identified as strong inhibitors of c-type lysozymes.[7,8,11−13] MliC/PliC is more widely distributed in Gram-negative bacteria than Ivy or Ivy-like proteins. Strong inhibitors of i-type or g-type lysozymes are also found in some Gram-negative bacteria and are named PliI (periplasmic lysozyme inhibitor of i-type lysozyme) and PliG (periplasmic lysozyme inhibitor of g-type lysozyme).[9,10]

Because lysozyme inhibitors are essential for the survival of the pathogenic Gram-negative bacteria in animal hosts, they are an interesting target for the development of novel antibacterial agents. To this end, it is important to understand how these inhibitors recognize the cognate lysozymes at the atomic level. The complex structure of Ivy from *Escherichia coli* and c-type lysozyme from chicken egg white (HEWL) has been determined by X-ray crystallography.[12] The crystal structure of MliC from *Pseudomonas aeruginosa* (named *Pa*MliC in this study) in complex with HEWL revealed that the inhibition mechanism was characterized as a double-key lock.[14] A similar double-key lock interface was also observed in the complex structure of PliG from *E. coli* and a g-type lysozyme from salmon.[15]

Brucella spp. are Gram-negative bacteria and function as facultative intracellular parasites causing brucellosis of animals such as cattle, dogs, and humans.[16] *Brucella abortus* is the principal cause of brucellosis in cattle, and the infected cattle show a high incidence of abortions.[17] However, *B. abortus* is not a significant pathogen in avian species.[18] Brucellosis in humans is usually associated with ingestion of unsterilized milk or meat from infected animals. *B. abortus* has a lysozyme inhibitor against the c-type lysozyme, which might be responsible for counteracting the c-type lysozyme of the host animals, and thus may function as a colonization or virulence factor in the bacteria.

Received: September 7, 2013
Revised: December 5, 2013
Published: December 5, 2013

dx.doi.org/10.1021/bi401241c | *Biochemistry* 2013, 52, 9385−9393

Here, we present the crystal structures of PliC from *B. abortus* and its complex structure with human c-type lysozyme (hLYZ) at high resolution. The structures give a detailed account of the molecular mechanism of lysozyme inhibition by PliC from *B. abortus*.

MATERIALS AND METHODS

Overexpression and Purification of the *B. abortus* PliC Protein. DNA fragments encoding *B. abortus* PliC (mature form, residues 27−121) were amplified from the genomic DNA from *B. abortus* using the polymerase chain reaction method and ligated into the NcoI and XhoI sites of the pProEX-HTA vector (Invitrogen). *Ba*PliC protein was recombinantly expressed in *E. coli* BL21(DE3). Cells were cultured in 3 L of LB medium at 37 °C, and the protein was induced at an OD_{600} of 0.7 by adding IPTG (final concentration of 1 mM). *Ba*PliC protein was produced as an inclusion body, and the inclusion body proteins were in 40 mL of 20 mM sodium acetate (pH 4.6) buffer containing 6 M urea and 10 mM 2-mercaptoethanol. After the insoluble materials had been removed by centrifugation, the supernatant fluid (40 mL) was dialyzed two times against 1 L of 20 mM Tris (pH 8.0) buffer containing 5 mM 2-mercaptoethanol at 4 °C. Then the solution was further dialyzed against 1 L of 20 mM Tris (pH 8.0) buffer overnight at 4 °C. The protein was purified from the solubilized proteins by Ni-NTA affinity chromatography. The hexahistidine tag was removed from the protein by overnight treatment of TEV protease in the presence of 5 mM 2-mercaptoethanol. The PliC protein was further purified using a Hitrap-Q anion exchange column. Finally, the fractions containing PliC were applied to a HiLoad Superdex 16/60 200 column (GE Healthcare), equilibrated with 20 mM Tris (pH 8.0) buffer containing 150 mM NaCl. The purified proteins were concentrated (final concentration of 15 mg/mL) using Centriprep (Millipore) and stored frozen at −80 °C until they were used. The protein concentration was determined by measuring the absorbance at 280 nm based on the molar extinction coefficient (20065 M^{-1} cm^{-1}). To obtain the *Ba*PliC−hLYZ complex, the purified *Ba*PliC protein was mixed with an excess of human lysozyme (Sigma), and then the complex was purified with a HiLoad Superdex 16/60 200 column (GE Healthcare).

Crystallization, Collection of Data, and Determination of the Structure of the *Ba*PliC Orthorhombic Form. *Ba*PliC (orthorhombic form) protein (15 mg/mL) was crystallized in a precipitation solution containing 1.9 M ammonium sulfate, 0.1 M Tris-HCl (pH 8.5), and 10% (v/v) glycerol at 14 °C. X-ray diffraction data of the crystals were collected at beamline 5C of the Pohang Accelerator Laboratory (PAL) using a QUANTUM 270 CCD detector (ADSC). The diffraction data sets were handled and scaled with the HKL2000 package.[19] The crystal belonged to space group $P2_12_12_1$ with the following cell dimensions: a = 91.2 Å, b = 64.4 Å, and c = 47.6 Å. Initial phases were determined by the molecular replacement package MOLREP[20] using the coordinates of *Salmonella typhimurium* MliC [Protein Data Bank (PDB) entry 3F6Z] as a search model. Coot was used afterward to complete the model manually,[21] and model refinement was conducted using PHENIX.[22]

Crystallization, Collection of Data, and Determination of the Structure of *Ba*PliC in the Hexagonal Crystal Form. Crystals of *Ba*PliC (hexagonal form) were obtained by the same method as *Ba*PliC (orthorhombic form). The best crystals of *Ba*PliC (hexagonal form) were obtained by mixing 1 μL of the protein solution with 1 μL of the precipitant solution with 0.1 M sodium acetate (pH 4.6) and 2.0 M ammonium sulfate. Data sets were collected as described above, and the crystal belonged to space group $P6_122$ with the following cell dimensions: a = 58.4 Å, b = 58.4 Å, and c = 364.8 Å. Initial phases were determined by the molecular replacement package MOLREP[20] using coordinates of the *Ba*PliC (orthorhombic form) structure as a search model.

Crystallization, Collection of Data, and Determination of the Structure of the *Ba*PliC−hLYZ Complex. The optimal PliC−HLZ complex crystals were obtained by mixing 1 μL of the protein solution in a 1:1 ratio with 0.1 M sodium citrate tribasic (pH 5.6) and 40% (v/v) *tert*-butanol. The crystal belongs to space group $P2_12_12$ with the following cell dimensions: a = 100.3 Å, b = 89.0 Å, and c = 66.2 Å. Initial phases were determined by the molecular replacement package MOLREP using the coordinates of hLYZ (PDB entry 1JKB) as a search model. The model was obtained by the same method as PliC. Crystallographic data statistics are summarized in Table 1. All figures were prepared with PYMOL.[23]

Table 1. X-ray Data Collection and Refinement Statistics

	*Ba*PliC (orthorhombic form)	*Ba*PliC (hexagonal form)	*Ba*Plic−hLYZ complex
Data Collection			
source	BL 5C (PLS)	BL 5C (PLS)	BL 5C (PLS)
wavelength (Å)	0.9795	0.9793	0.9795
resolution limit (Å)	50−2.0	20−2.3	50−1.8
space group	$P2_12_12_1$	$P6_122$	$P2_12_12$
unit cell (Å)	a = 91.2, b = 64.4, c = 47.6	a = 58.4, b = 58.4, c = 364.8	a = 100.3, b = 89, c = 66.2
redundancy	6.8 (3.7)[a]	12.0 (7.3)[a]	10.4 (9.3)[a]
R_{sym} (%)	8.9 (23.1)[a]	2.0 (7.2)[a]	2.9 (5.3)[a]
completeness (%)	96.1 (87.7)[a]	98.5 (97.5)[a]	96.8 (99.8)[a]
I/σ	24.4 (4.1)[a]	28.5 (5.7)[a]	56.1 (11.4)[a]
Refinement			
resolution range (Å)	19−2.0	20−2.3	20−1.8
R factor (%)	21.5	20.3	18.5
R_{free} (%)[b]	26.4	27.0	22.2
average B value (Å^2)	18.04	21.31	17.70
Wilson B factor (Å^2)	22.55	34.68	18.41
root-mean-square deviation for bonds (Å)	0.008	0.008	0.007
root-mean-square deviation for angles (deg)	1.093	1.155	1.109
Ramachandran plot (%)			
most favored	98.96	93.31	97.82
additionally favored	1.04	6.34	2.18
coordinate error (Å)	0.26	0.35	0.18
PDB entry	4MIS	4MIR	4ML7

[a]The numbers in parentheses are statistics for the highest-resolution shell. [b]R_{free} was calculated with 5% of the data set.

Size-Exclusion Chromatography. To determine the molecular weights of proteins, size-exclusion chromatography was performed at a flow rate of 0.5 mL/min on Superdex S-200 HR 10/30 column (GE Healthcare) equilibrated with 20 mM Tris buffer (pH 8.0) containing 150 mM NaCl.

Isothermal Titration Calorimetry. Isothermal titration calorimetry (ITC) measurements were performed on a

dx.doi.org/10.1021/bi401241c | *Biochemistry* 2013, 52, 9385−9393

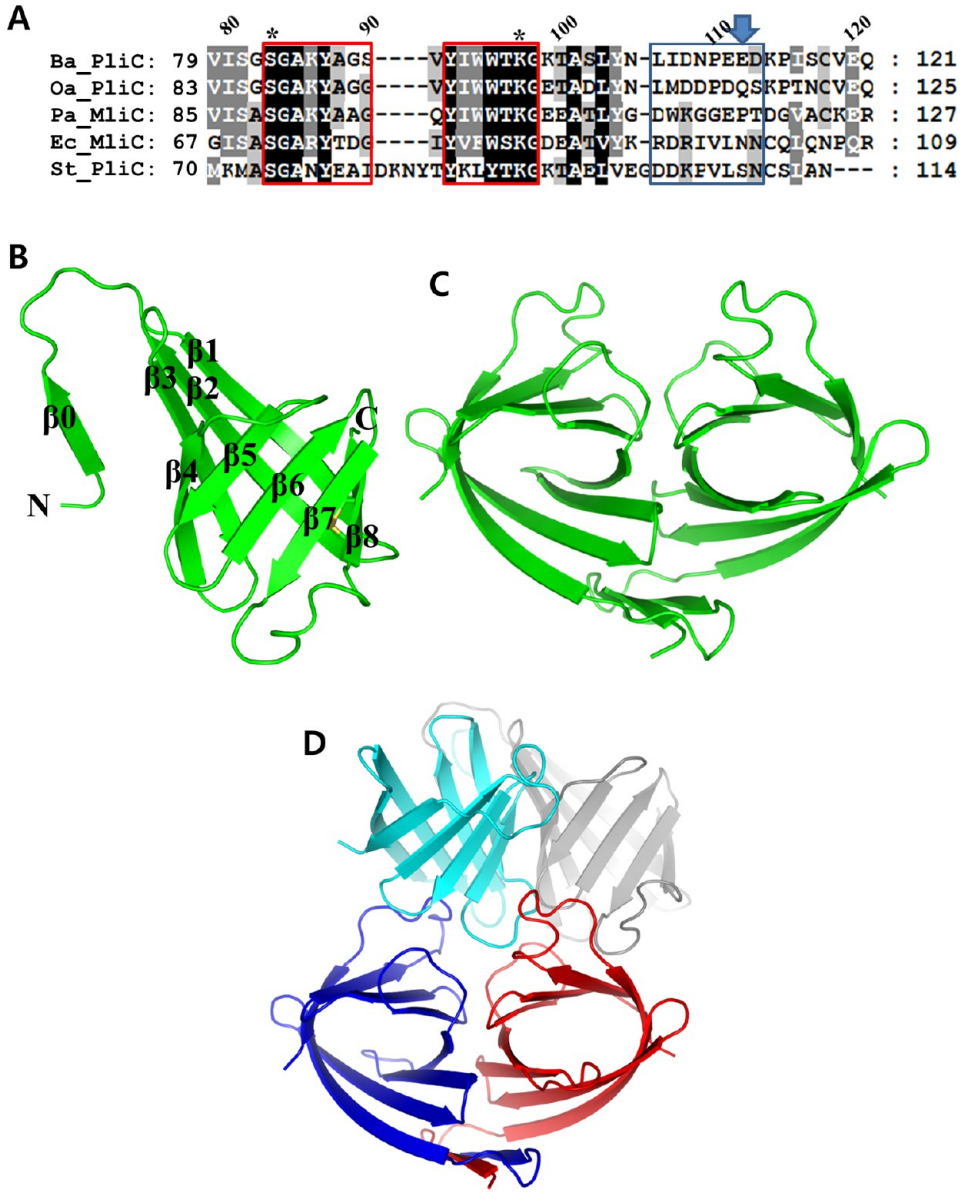

Figure 1. Overall structures of *Ba*PliC. (A) Sequence alignment of the C-terminal part of MliC/PliC proteins. The key conserved regions are shown in red boxes, and the putative signal sequences are highlighted in gray. In the key conserved regions, Ser83 and Lys97 are denoted with asterisks. The E112 loop is shown in a blue box, and Glu112 is denoted with a blue arrow. The alignment was performed using CLUSTALX.[29] (B) Structure of a *Ba*PliC protomer in the asymmetric unit in the orthorhombic crystal form. Secondary structural elements are numbered. The disulfide bridge between Cys47 and Cys108 is shown as sticks. (C) Asymmetric unit of *Ba*PliC in the orthorhombic crystal form, displayed as ribbons. (D) Structure of *Ba*PliC in the hexagonal crystal form, displayed as ribbons. The asymmetric unit contains three protomers colored red, blue, and cyan. The molecule colored gray was generated by crystallographic 2-fold symmetry using the protomer that is colored cyan.

Microcal (GE Healthcare) VP-ITC microcalorimeter, typically at 25 °C. ITC was used to probe the interaction between the the *Ba*PliC wild-type protein or the E112A variant protein and HEWL or hLYZ. All the proteins used in these experiments were dialyzed into 20 mM Hepes (pH 7.5) and 150 mM NaCl, and then the sample was concentrated (final concentration of 10 μM) using an ultrafiltration device. Both the protein and the titrant solutions were thoroughly degassed in a ThermoVac apparatus (Microcal). For a titration experiment, approximately 2 mL of the protein solution was placed in a reaction cell and the contents of the reaction cell were continuously stirred at 300 rpm while 25 injections were made (10 μL each). Data analysis was performed by nonlinear regression fitting to the sequential binding model using Origin (Microcal). Association constant K_A, enthalpy change ΔH, and the stoichiometry were obtained from fitting the data.[24]

RESULTS

Determination of the Structure of *B. abortus* PliC. We found a candidate for the inhibitor against c-type lysozyme from *B. abortus* in GenBank, which was annotated as MliC. In this study, it is designated as PliC because this gene was not predicted to have the membrane anchoring sequence, called lipobox, at the N-terminus. On the basis of a sequence comparison with MliC/PliC family proteins, PliC likely belongs to a dimeric family of MliC/PliC like *Pa*MliC[14] (Figure 1A). A mature form of PliC from *B. abortus* (*Ba*PliC) was recombinantly expressed in *E. coli* as an inclusion body, from

dx.doi.org/10.1021/bi401241c | *Biochemistry* 2013, 52, 9385−9393

which the functional protein was purified to homogeneity using the refolding method. Size-exclusion chromatography indicated that *Ba*PliC forms a tetrameric or higher-order oligomer in 20 mM Tris buffer (pH 8.0) containing 150 mM NaCl and 2 mM 2-mercaptoethanol (Figure S1 of the Supporting Information). We obtained crystals in two different crystal forms (orthorhombic and hexagonal crystal forms) and determined the crystal structures of both crystal forms.

The structure of the orthorhombic crystal form was determined by the molecular replacement method using the dimeric unit of the *Pa*MliC coordinates in the *Pa*MliC−HEWL complex structure (PDB entry 3F6Z)[14] as a search model. Then, the structure of the hexagonal crystal form was determined using the structure of *Ba*PliC in the orthorhombic crystal form. One dimeric unit was contained in the asymmetric unit of the orthorhombic crystal form, while one dimeric unit and one monomeric unit were present in the hexagonal crystal form (Figure 1). Considering the crystal contact in the hexagonal crystal form, the monomeric unit forms the identical dimer by interaction with the neighboring molecule that is related by the crystallographic 2-fold axis (Figure 1D). The Matthews coefficients (V_m) of the orthorhombic and hexagonal crystals were 2.95 and 1.97 Å^3/Da, respectively, and the solvent contents were calculated to be 58 and 38%, respectively.

The final models of the orthorhombic and hexagonal crystal forms were refined against the 2.0 and 2.3 Å resolution data sets, respectively. All 95 residues could be built into the electron density with the cloning artifact (Met-Gly amino acid sequence) at the N-terminus. Further details about the determination of the structure and refinement are given in Table 1.

Overall Structure of *B. abortus* PliC and Its Comparison with That of *P. aeruginosa* MliC. The overall structures of the two *Ba*PliC coordinates in the different crystal forms are very similar with minor variations [Figure S2 of the Supporting Information; root-mean-square deviation (rmsd) of 0.44 Å for 163 Cα atoms]. The crystal structures revealed that each protomer has a slightly flattened β-barrel that consists of eight antiparallel β-strands (β1−β8) and is stabilized by a disulfide bridge between Cys47 and Cys108, located at the ends of the first (β1) and eighth strands (β8) of the barrel, respectively (Figure 1A and Figure S2 of the Supporting Information). This β-barrel is a common core structural motif among all MliC/PliC family proteins, including *E. coli* and *S. typhimurium* PliC.[25,26] However, the N-terminal region of *Ba*PliC has an additional β-strand (β0) interacting between the protomers in an intermolecular manner, leading to an extensive dimeric interface as observed in *Pa*MliC[14] (Figure 2A). The hydrophobic residues and interactions in the dimeric interfaces are well-conserved in *Ba*PliC like *Pa*MliC (Figure 2A).

Structural superposition of *Ba*PliC on *Pa*MliC revealed that *Ba*PliC has a protruding loop (named the E112 loop in this study) between β7 and β8, whose amino acid sequence is variable among the MliC/PliC family proteins (Figures 1A and 2B). While the loop is well-ordered in the *Ba*PliC structure, the corresponding region in the *Pa*MliC structure is largely disordered (Figure 2B; see below for the role of the loop). Additionally, sequence and structural analyses revealed that *Pa*MliC has a longer N-terminal extension region, which is associated with the membrane anchoring of MliC proteins (Figure 2B). The long N-terminal extension, together with the cysteine-linked lipid moiety, might be involved in the membrane anchoring of the MliC proteins. Because PliC is not anchored to the membrane, the N-terminal extension region might be evolutionarily degenerated.

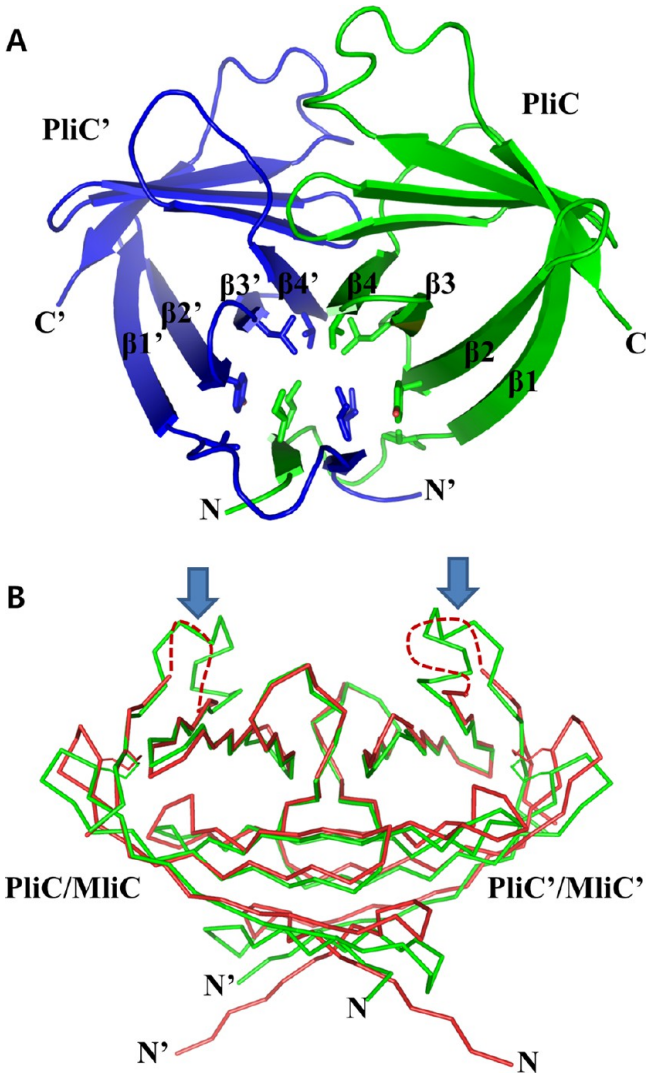

Figure 2. Structural comparison of *B. abortus* PliC with *P. aeruginosa* MliC. (A) Dimeric interface of *Ba*PliC observed in the orthorhombic crystal form. A hydrophobic surface is found on the outer face of β0 and β2−β4. The hydrophobic surface consists of Val38, Tyr57, Leu64, and Val75 from each protomer and Ile28 and Ile30 from the other protomers, which play an important role in dimer formation. The residues on the hydrophobic surface are conserved only among the subgroup 2 MliC/PliC proteins. In the ribbon representation, the hydrophobic residues are drawn as sticks. (B) Structural superposition of the Cα traces of *Ba*PliC (green) and *Pa*MliC (red). The structure of *Pa*MliC was taken from its complex structure with HEWL (PDB entry 3F6Z). The *Ba*PliC structure in the orthorhombic crystal form was used as a representative structure of *Ba*PliC. The disordered regions are shown with dashed lines. The E112 loops are denoted with arrows. The two *Ba*PliC/*Pa*MliC molecules are labeled PliC/MliC and PliC′/MliC′, respectively.

Overall Structure of *B. abortus* PliC in Complex with Human Lysozyme. The crystal structure of *Ba*PliC in complex with its cognate lysozyme is required for the analysis of the binding interface of *Ba*PliC at the atomic level. After *Ba*PliC and hLYZ proteins had been mixed in equimolar amounts, the stable complex of *Ba*PliC and hLYZ was purified by size-exclusion chromatography. Size-exclusion chromatography showed that the purified protein forms a tight complex

dx.doi.org/10.1021/bi401241c | *Biochemistry* 2013, 52, 9385−9393

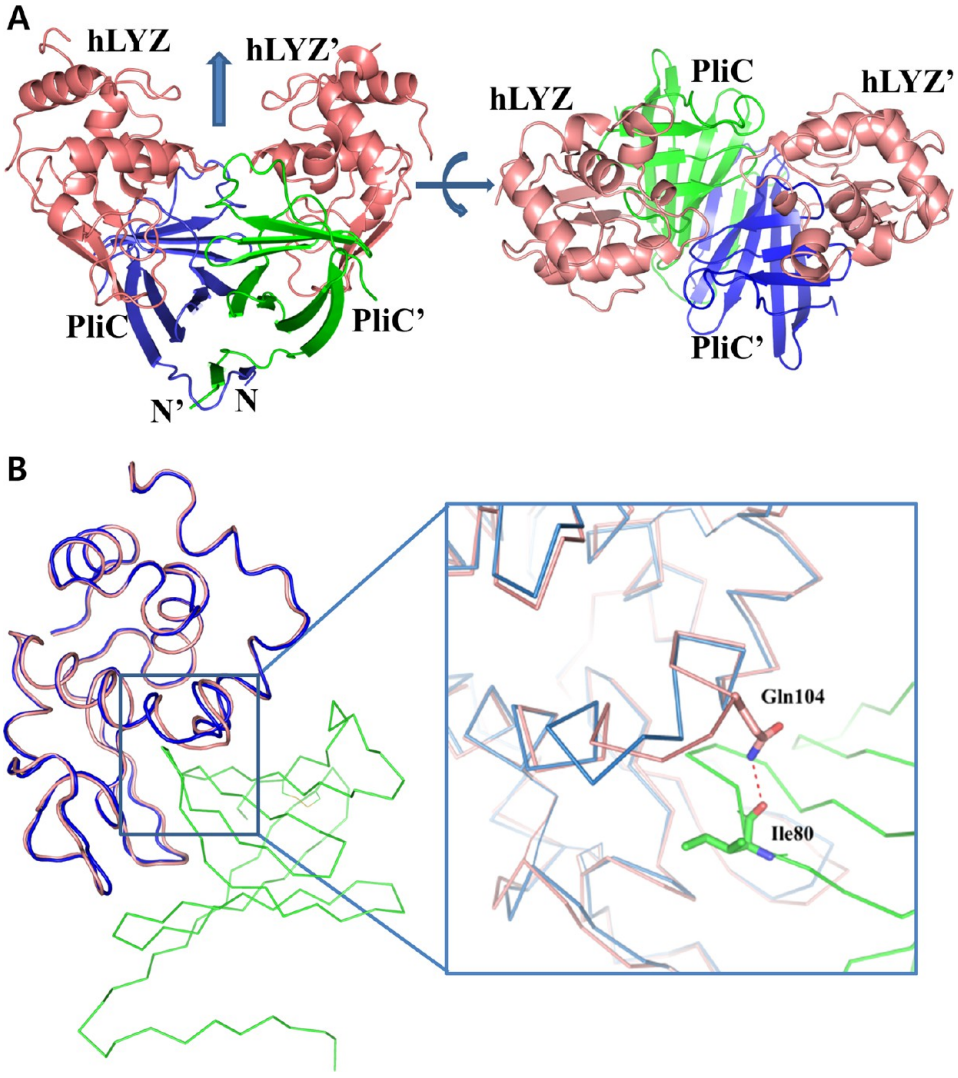

Figure 3. Overall structure of *Ba*PliC in complex with hLYZ. (A) Asymmetric unit of the *Ba*PliC−hLYZ complex crystal, shown as ribbons. A side view is shown at the left and a top view at the right. The two lysozyme molecules are labeled hLYZ and hLYZ′, and the two *Ba*PliC molecules are labeled PliC and PliC′. The noncrystallographic 2-fold axis is indicated by an arrow (left). (B) Structural comparison of Cα traces of hLYZ in the free form (PDB entry 1JKB) and in complex with *Ba*PliC. hLYZ in the free form is colored blue, and the complex form with *Ba*PliC is colored pale red. *Ba*PliC is colored green. The key different region is denoted by the blue box. In the close-up, Gln104 of hLYZ forms a hydrogen bond with the backbone carbonyl group of Ile80 of *Ba*PliC; the hydrogen bond is shown as a dashed line.

with hLYZ (Figure S3 of the Supporting Information). High-quality crystals were obtained through screening and optimization of the crystallization conditions for the complex. The structure of the protein complex was determined by the molecular replacement method using the structure of the *Pa*MliC−HEWL complex[14] as a search model. The resulting model of the *Ba*PliC−hLYZ complex consists of 226 residues, comprising 100% of the total number of amino acid residues, and was refined to the 1.8 Å resolution data set with an R_{free} of 22.2%, which exhibits more detailed features than the structure of the *Pa*MliC−HEWL complex (2.3 Å resolution; R_{free} = 28.2%). The Matthews coefficient (V_m) of the crystal is 2.95 Å^3/Da, and the solvent content was calculated to be 58%.

The asymmetric unit of the crystal contains two *Ba*PliC molecules and two hLYZ molecules, probably representing their native complex in solution (Figure 3A). The overall shape resembles a heart symbol, as observed in the structure of the *Pa*MliC−HEWL complex[14] (Figure S4 of the Supporting Information). The two *Ba*PliC protomers form a dimer, and each *Ba*PliC protomer binds one hLYZ molecule. No physical interactions are present between the two hLYZ molecules in the complex structure, as observed in the structure of the *Pa*MliC−HEWL complex.

A comparison of the refined structure of *Ba*PliC in complex with hLYZ and that of free *Ba*PliC does not reveal any significant structural change (rmsd of 0.48 Å based on the Cα superimposition of 165 residues) (Figure S5 of the Supporting Information). When the structures of hLYZ and HEWL are superposed, the overall structures are very similar except for this active site lid region, in which Gln104 of hLYZ forms a hydrogen bond with the backbone carbonyl group of *Ba*PliC (Figure 3B). This interaction may cause the structural difference between the two lysozymes [rmsd of 0.33 Å (Figure 3B)]. These observations suggest that the interaction between the proteins does not cause the mutual conformational change of the proteins.

Major Binding Interface between *Ba*PliC and hLYZ. The complex structure revealed the key binding interfaces of

dx.doi.org/10.1021/bi401241c | *Biochemistry* 2013, 52, 9385−9393

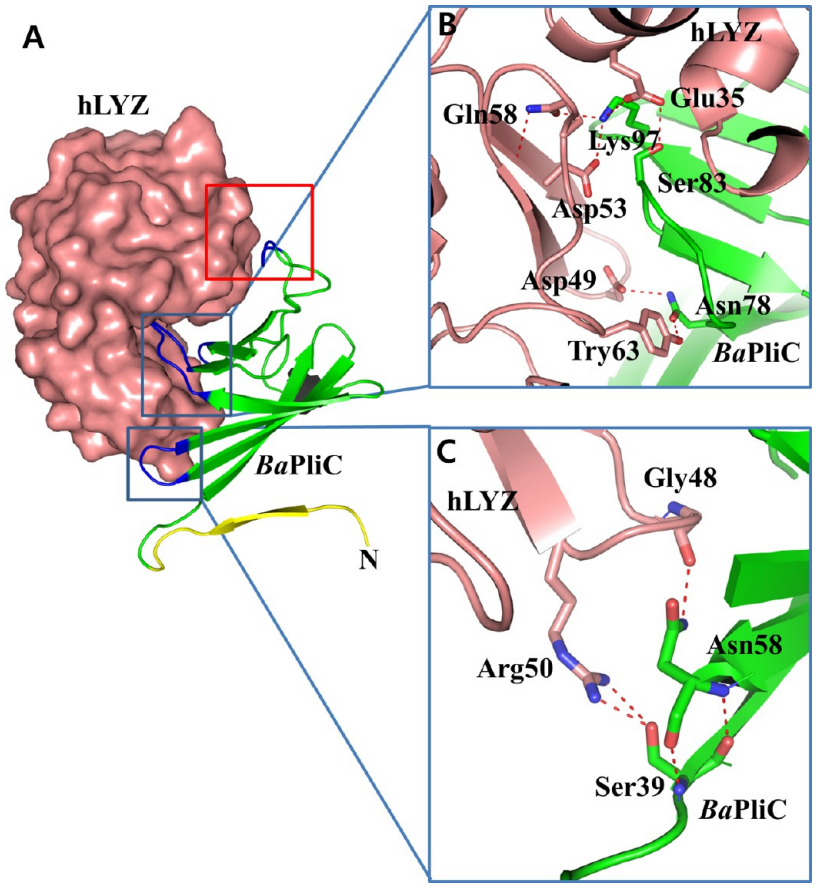

Figure 4. Major binding interface. (A) The active site cleft of hLYZ is occupied by the key conserved regions of *Ba*PliC. hLYZ is displayed as a pale red surface representation, and *Ba*PliC is shown as green ribbons, where the key conserved regions are shown in blue boxes. The N-terminal linker region is colored yellow. The unique binding interface is shown in a red box (see Figure 5A for the detail). (B) Close-up of the interaction between the catalytic residues of hLYZ and the key conserved regions of *Ba*PliC. hLYZ is colored pale red and *Ba*PliC green. At the left, Glu35, Asp53, and Gln58 of hLYZ and Ser83 and Lys97 in the key conserved regions of *Ba*PliC are displayed as sticks. Salt bridges and polar interactions are shown as dashed lines. At the right, Asn78 of *Ba*PliC forms hydrogen bonds with Asp49 and Try63 of hLYZ. Hydrogen bonds are shown as dashed lines. (C) Close-up of the interactions between hLYZ and the shallow pocket region of *Ba*PliC. hLYZ is colored pale red and *Ba*PliC green. Arg50 of hLYZ forms a hydrogen bond with Ser39 of *Ba*PliC. Asn58 of *Ba*PliC forms a polar interaction with the backbone carbonyl group of Gly48 of hLYZ. Hydrogen bonds and polar interactions are shown as dashed lines.

*Ba*PliC with hLYZ, providing a more detailed feature than the structure of the *Pa*MliC−HEWL complex because of the higher resolution. Overall, *Ba*PliC and hLYZ engage in a double-key lock interaction as observed in the complex structure of *Pa*MliC and HEWL (Figure 4). The active site cleft of hLYZ is entirely blocked by *Ba*PliC like a wedge consisting of the key conserved residues (Figure 4A and Figure S2 of the Supporting Information). Approximately 90% of the active site cleft area of hLYZ is covered by *Ba*PliC. The crystal structure clearly shows that the active site cleft is no longer accessible to substrate (Figure 4A).

The crystal structure showed that both surface and interior faces of β4−β6 of the β-barrel are the main binding interface of *Ba*PliC. Most residues in this region are strictly conserved among MliC/PliC family proteins and are involved in the interaction with lysozymes. Extensive polar interaction networks are found between the active site residues of hLYZ and the conserved residues Ser83 and Lys97 of *Ba*PliC, which block the active site cleft of the lysozyme (Figure 4B). Ser83 of *Ba*PliC engages in a polar interaction with Glu35 of the lysozyme, which forms a salt bridge with Lys97 of *Ba*PliC (Figure 4B). Lys97 of *Ba*PliC also forms a polar interaction with Asp53 and Gln58 of the lysozyme (Figure 4B). In addition, Tyr63 of the lysozyme forms a hydrogen bond with Asn78 of *Ba*PliC, and in turn, Asn78 of *Ba*PliC forms a hydrogen bond with Asp49 of the lysozyme (Figure 4B). Because these interactions are between the conserved residues of the two proteins, these interactions would be shared in *Ba*PliC and other c-type lysozymes.

In the structure of the HEWL−*Pa*MliC complex, a polar interaction between Thr102 and Tyr92 was observed in the shallow pocket region of *Pa*MliC.[14] In the hLYZ−*Ba*PliC complex, an equivalent interaction was observed between Asn58 of *Ba*PliC and the backbone carbonyl group of Gly48 of hLYZ (Figure 4C). Additionally, Arg50 of hLYZ forms a hydrogen bond with Ser39 of *Ba*PliC in hLYZ and *Ba*PliC (Figure 4C).

A Unique Binding Interface of *Ba*PliC with hLYZ. We found another contact between *Ba*PliC and hLYZ that involves the E112 loop of *Ba*PliC and the active site lid region of hLYZ. Salt bridges between Glu112 of *Ba*PliC and Arg107 and Arg113 of hLYZ were observed only in the structure of the *Ba*PliC−hLYZ complex (Figure 5A). This interaction seems to be unique in the structure of the *Ba*PliC−hLYZ complex because the corresponding region of *Pa*MliC is disordered in the crystal structure (Figure 5A),[14] and the Glu112 is replaced with

dx.doi.org/10.1021/bi401241c | *Biochemistry* 2013, 52, 9385−9393

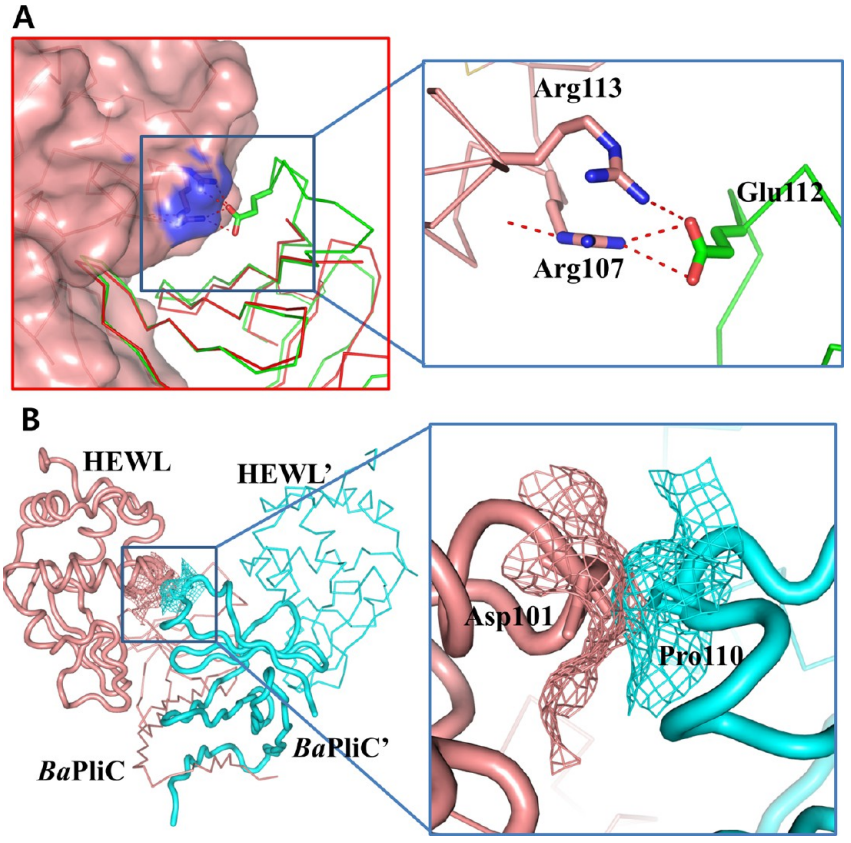

Figure 5. Unique binding interface. (A) Unique binding interface in *Ba*PliC and hLYZ. hLYZ is displayed as a pale red surface representation, and *Ba*PliC is displayed as green ribbons. In the close-up, Arg107 and Arg113 of hLYZ form salt bridges with Glu112 of *Ba*PliC, where the salt bridges are shown as dashed lines. (B) Docking model of HEWL and *Ba*PliC. HEWL is colored magenta and *Ba*PliC cyan. The putative steric clash occurs in the HEWL active site lid region and the E112 loop in *Ba*PliC′. In the docking model, Asp101 of HEWL and Pro110 of *Ba*PliC form a steric clash, displayed as mesh.

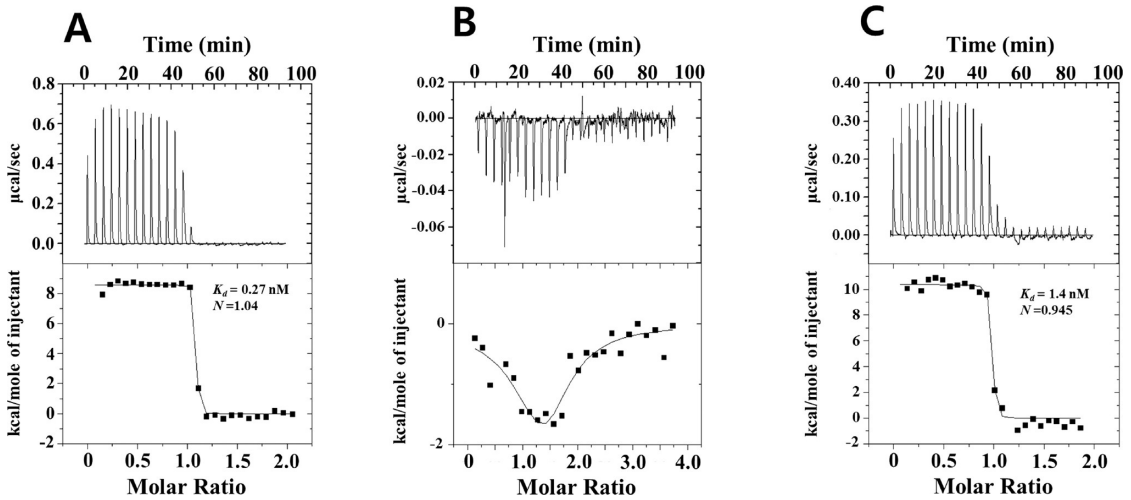

Figure 6. ITC analysis of the binding of *Ba*PliC to hLYZ and HEWL. (A) Measurement of the K_d of hLYZ with wild-type *Ba*PliC. Raw data output of power (heat released) for each of 25 consecutive injections of hLYZ (200 μM) into the wild-type *Ba*PliC protein (20 μM) at 25 °C is displayed in the top panel. (B) Measurement of the K_d of HEWL with wild-type *Ba*PliC. hLYZ (200 μM) was injected consecutively 25 times into the wild-type *Ba*PliC protein (20 μM) at 25 °C, and the raw data output of power (heat released) is displayed in the top panel. (C) Measurement of the K_d of hLYZ with *Ba*PliC variant E112A. hLYZ (200 μM) was injected consecutively 25 times into the *Ba*PliC E112A mutant protein (20 μM) at 25 °C, and the raw data output of power (heat released) is displayed in the top panel. In the bottom panels is shown heat exchange at each injection obtained by integration of each injection spike in the top panel, normalized to the number of kilocalories per mole of hLYZ or HEWL. The titration curve is the computer-generated best-fit model of sequential binding with four sites. The statistical result is given in Table 2.

proline in *Pa*MliC (Figure 1A). Moreover, a steric clash was observed when HEWL was docked onto the *Ba*PliC structure at this active site lid region of the other molecule of HEWL because of the structural difference in the active site lid region

dx.doi.org/10.1021/bi401241c | *Biochemistry* 2013, 52, 9385−9393

Table 2. ITC Measurements of Binding of *Ba*PliC WT or E112A to hLYZ or HEWL

*Ba*PliC	lysozyme	temp (K)	K_d	ΔH (kcal/mol)	$T\Delta S$ (kcal/mol)	ΔG (kcal/mol)
WT	hLYZ	298	0.27 nM	8.59	21.6	−13.0
E112A	hLYZ	298	1.4 nM	10.38	22.4	−12.02
WT						
site 1	HEWL	298	0.21 μM	0.018	9.15	−9.15
site 2	HEWL	298	1.1 μM	−27.24	−19.08	−8.6

between hLYZ and HEWL (Figure 5B). Taken together, our findings suggest that *Ba*PliC is more suited for inhibition of hLYZ than HEWL.

Tighter Binding of *Ba*PliC to hLYZ Than to HEWL. We next measured the binding affinities between *Ba*PliC and hLYZ using ITC. A typical sigmoidal endothermic peak pattern was observed when hLYZ was used as a titrant, indicating strong binding between *Ba*PliC and hLYZ. From the results, the K_d value was 0.27 nM, indicating that *Ba*PliC forms a very tight complex with hLYZ with a 1:1 stoichiometry between the protomers of the proteins (Figure 6A). This observation is comparable to the previously established high affinity of PliG and SalG (K_d = 1.7 nM), as determined by a surface plasmon resonance experiment.[9]

To compare the binding affinity of *Ba*PliC for hLYZ with that for HEWL, we also performed the ITC experiment with HEWL. In contrast to hLYZ, HEWL generated an exothermic binding pattern with a sharp bend (Figure 6B), indicating that the binding modes of *Ba*PliC and HEWL are significantly different. The integrated peaks were fit to the sequential binding model, yielding K_d values of 0.21 and 1.1 μM. These results suggest that the binding at one protomer of the *Ba*PliC dimer affects binding at the other protomer. Most importantly, the binding affinity of *Ba*PliC for HEWL was drastically lower compared to the affinity to hLYZ. This finding is in line with the salt bridge that is only found in *Ba*PliC and hLYZ and the structural docking experiment with *Ba*PliC and HEWL, shown in Figure 3B.

To assess the role of the ionic pair of Glu112 of *Ba*PliC and Arg113 of hLYZ in the specific inhibition of hLYZ, we generated a *Ba*PliC variant with an E112A mutation and measured the K_d of the mutant protein with hLYZ (Figure 6C). As shown in Table 2, the mutation weakened the abilities to bind hLYZs by 5-fold. These results indicate that the unique salt bridge between *Ba*PliC and hLYZ is responsible for their tighter binding and that *Ba*PliC evolved to more efficiently inhibit hLYZ, discriminating the slight structural difference between human and chicken c-type lysozymes.

DISCUSSION

To date, only non-human lysozymes have been characterized in terms of inhibition by the lysozyme inhibitory proteins. Previously, the physical interaction between MliC/PliC from *P. aeruginosa* and HEWL was described at moderate resolution.[14] In this study, we present crystal structures of *Ba*PliC alone and in complex with hLYZ. The structure of *Ba*PliC alone shows a dimeric interface similar to that of *Pa*MliC but different from that of PliC from *S. typhimurium*. Because of the higher resolution, the structure of the *Ba*PliC−hLYZ complex displayed better features than that of the *Pa*MliC−HEWL complex previously reported.[14] The structure revealed that the conserved loop of *Ba*PliC was inserted into the active site of lysozyme via extensive interactions, as in the structure of the *Pa*MliC−HEWL complex.[14] Furthermore, we found that a unique interaction was mediated by a loop carrying Glu112 in *Ba*MliC (E112 loop) and a loop carrying Pro103 in hLYZ. The corresponding loops of *Pa*MliC and HEWL were disordered or displayed a different conformation. Mutational study further suggested that the E112 loop of *Ba*PliC was also involved in the recognition of hLYZ.

The crystal structure and the ITC experiments provided important information in the development of agents that suppress the action of the MliC/PliC family proteins. Considering the K_d value between *Ba*PliC and the human lysozyme, the off rate between the two proteins would be very slow. The shallow pocket of the MilC/PliC family proteins and the strong interaction between the inhibitory protein and the lysozyme indicate that the shallow pocket of MliC/PliC proteins might not be a good target for developing drug candidates that can interfere with the binding between MliC/PliC and lysozymes.

Protein engineering of human lysozyme has been used to attempt to improve the antimicrobial activity of the lysozyme.[27,28] The high-resolution structure of *Ba*PliC and hLYZ may provide a direction for how the lysozyme can be engineered to prevent its inhibition by the MliC/PliC family proteins of Gram-negative bacteria. The entrance to the active site, exhibiting the greatest structural difference from HEWL, might be a good target site for engineering because the residues are not directly involved in the catalysis of the enzyme but are important for binding to MliC/PliC. Thus, the engineered lysozymes in these regions could exhibit enhanced bactericidal activity without inhibiting the MliC/PliC family proteins of pathogens.

In summary, we determined the crystal structures of *Ba*PliC alone and in complex with human lysozyme. The crystal structure revealed how *Ba*PliC strongly and specifically inhibits human lysozymes compared with a homologous lysozyme from chicken. Our study has improved the understanding of bacterium−host interactions by revealing the interface of a lysozyme inhibitor to lysozyme. Furthermore, the structures and mechanism of action of MliC/PliC will be relevant to the control of bacterial growth in animal hosts, because MliC/PliC family members have been implicated as putative colonization or virulence factors.

ASSOCIATED CONTENT

Supporting Information

Experimental procedures and additional data. This material is available free of charge via the Internet at http://pubs.acs.org.

AUTHOR INFORMATION

Corresponding Author

*Room #311, Pharmacy Building, Pusan National University, Busandaehak-ro, Geumjeong-gu, Busan 609-735, Republic of Korea. Telephone: +82 51 510 2528. Fax: +82 51 513 6754. E-mail: hnc@pusan.ac.kr.

Author Contributions

S.-H.U. and J.-S.K. contributed equally to this work.

Funding

This research was financially supported by the Ministry of Knowledge Economy (MKE), Korea Institute for Advancement of Technology (KIAT), through the Inter-ER Cooperation Projects (R0000577).

Notes

The authors declare no competing financial interest.

■ ACKNOWLEDGMENTS

This study required the use of beamline 5C at Pohang Accelerator Laboratory (Pohang, Korea).

■ REFERENCES

(1) Fleming, A. (1922) On a remarkable bacteriolytic element found in tissues and secretions. *Proc. R. Soc. London, Ser. B 93*, 306−317.

(2) Prager, E. (1996) *Animal Lysozymes c and g: An Overview*, Birkhauser, Basel, Switzerland.

(3) Jolles, P., and Jolles, J. (1984) What's new in lysozyme research? Always a model system, today as yesterday. *Mol. Cell. Biochem. 63*, 165−189.

(4) Callewaert, L., and Michiels, C. W. (2010) Lysozymes in the animal kingdom. *J. Biosci. 35*, 127−160.

(5) Bellamy, W., Takase, M., Wakabayashi, H., Kawase, K., and Tomita, M. (1992) Antibacterial spectrum of lactoferricin B, a potent bactericidal peptide derived from the N-terminal region of bovine lactoferrin. *J. Appl. Bacteriol. 73*, 472−479.

(6) Bellamy, W. R., Wakabayashi, H., Takase, M., Kawase, K., Shimamura, S., and Tomita, M. (1993) Role of cell-binding in the antibacterial mechanism of lactoferricin B. *J. Appl. Bacteriol. 75*, 478−484.

(7) Callewaert, L., Aertsen, A., Deckers, D., Vanoirbeek, K. G., Vanderkelen, L., Van Herreweghe, J. M., Masschalck, B., Nakimbugwe, D., Robben, J., and Michiels, C. W. (2008) A new family of lysozyme inhibitors contributing to lysozyme tolerance in Gram-negative bacteria. *PLoS Pathog. 4*, e1000019.

(8) Monchois, V., Abergel, C., Sturgis, J., Jeudy, S., and Claverie, J. M. (2001) *Escherichia coli ykfE* ORFan gene encodes a potent inhibitor of C-type lysozyme. *J. Biol. Chem. 276*, 18437−18441.

(9) Vanderkelen, L., Van Herreweghe, J. M., Vanoirbeek, K. G., Baggerman, G., Myrnes, B., Declerck, P. J., Nilsen, I. W., Michiels, C. W., and Callewaert, L. (2011) Identification of a bacterial inhibitor against g-type lysozyme. *Cell. Mol. Life Sci. 68*, 1053−1064.

(10) Van Herreweghe, J. M., Vanderkelen, L., Callewaert, L., Aertsen, A., Compernolle, G., Declerck, P. J., and Michiels, C. W. (2010) Lysozyme inhibitor conferring bacterial tolerance to invertebrate type lysozyme. *Cell. Mol. Life Sci. 67*, 1177−1188.

(11) Pellegrini, A., Thomas, U., Bramaz, N., Klauser, S., Hunziker, P., and von Fellenberg, R. (1997) Identification and isolation of a bactericidal domain in chicken egg white lysozyme. *J. Appl. Microbiol. 82*, 372−378.

(12) Abergel, C., Monchois, V., Byrne, D., Chenivesse, S., Lembo, F., Lazzaroni, J. C., and Claverie, J. M. (2007) Structure and evolution of the Ivy protein family, unexpected lysozyme inhibitors in Gram-negative bacteria. *Proc. Natl. Acad. Sci. U.S.A. 104*, 6394−6399.

(13) Callewaert, L., Vanderkelen, L., Deckers, D., Aertsen, A., Robben, J., and Michiels, C. W. (2008) Detection of a lysozyme inhibitor in *Proteus mirabilis* by a new reverse zymogram method. *Appl. Environ. Microbiol. 74*, 4978−4981.

(14) Yum, S., Kim, M. J., Xu, Y., Jin, X. L., Yoo, H. Y., Park, J. W., Gong, J. H., Choe, K. M., Lee, B. L., and Ha, N. C. (2009) Structural basis for the recognition of lysozyme by MliC, a periplasmic lysozyme inhibitor in Gram-negative bacteria. *Biochem. Biophys. Res. Commun. 378*, 244−248.

(15) Leysen, S., Vanderkelen, L., Weeks, S. D., Michiels, C. W., and Strelkov, S. V. (2013) Structural basis of bacterial defense against g-type lysozyme-based innate immunity. *Cell. Mol. Life Sci. 70*, 1113−1122.

(16) Golding, B., Scott, D. E., Scharf, O., Huang, L. Y., Zaitseva, M., Lapham, C., Eller, N., and Golding, H. (2001) Immunity and protection against *Brucella abortus*. *Microbes Infect. 3*, 43−48.

(17) Samartino, L. E., and Enright, F. M. (1993) Pathogenesis of abortion of bovine brucellosis. *Comparative Immunology, Microbiology and Infectious Diseases 16*, 95−101.

(18) Detilleux, P. G., Cheville, N. F., and Deyoe, B. L. (1988) Pathogenesis of *Brucella abortus* in chicken embryos. *Vet. Pathol. 25*, 138−146.

(19) Otwinosky, Z., and Minor, W. (1997) Processing of X-ray diffraction data collected in oscillation mode. *Methods Enzymol. 276*, 307−326.

(20) Collaborative Computational Project, Number 4 (1994) The CCP4 suite: Programs for protein crystallography. *Acta Crystallogr. D50*, 760−763.

(21) Emsley, P., and Cowtan, K. (2004) Coot: Model-building tools for molecular graphics. *Acta Crystallogr. D60*, 2126−2132.

(22) Adams, P. D., Grosse-Kunstleve, R. W., Hung, L. W., Ioerger, T. R., McCoy, A. J., Moriarty, N. W., Read, R. J., Sacchettini, J. C., Sauter, N. K., and Terwilliger, T. C. (2002) PHENIX: Building new software for automated crystallographic structure determination. *Acta Crystallogr. D58*, 1948−1954.

(23) DeLano, W. (2002) *The PyMOL User's Manual*, DeLano Scientific, Palo Alto, CA.

(24) Wiseman, T., Williston, S., Brandts, J. F., and Lin, L. N. (1989) Rapid measurement of binding constants and heats of binding using a new titration calorimeter. *Anal. Biochem. 179*, 131−137.

(25) Revington, M., Semesi, A., Yee, A., Arrowsmith, C. H., and Shaw, G. S. (2006) The solution structure of the protein ydhA from *Escherichia coli*. *J. Biomol. NMR 35*, 295−300.

(26) Leysen, S., Van Herreweghe, J. M., Callewaert, L., Heirbaut, M., Buntinx, P., Michiels, C. W., and Strelkov, S. V. (2011) Molecular basis of bacterial defense against host lysozymes: X-ray structures of periplasmic lysozyme inhibitors PliI and PliC. *J. Mol. Biol. 405*, 1233−1245.

(27) Scanlon, T. C., Teneback, C. C., Gill, A., Bement, J. L., Weiner, J. A., Lamppa, J. W., Leclair, L. W., and Griswold, K. E. (2010) Enhanced antimicrobial activity of engineered human lysozyme. *ACS Chem. Biol. 5*, 809−818.

(28) Gill, A., Scanlon, T. C., Osipovitch, D. C., Madden, D. R., and Griswold, K. E. (2011) Crystal structure of a charge engineered human lysozyme having enhanced bactericidal activity. *PLoS One 6*, e16788.

(29) Thompson, J. D., Gibson, T. J., Plewniak, F., Jeanmougin, F., and Higgins, D. G. (1997) CLUSTALX windows interface: Flexible strategies for multiple sequence alignment aided by quality analysis tools. *Nucleic Acids Res. 25*, 4876−4882.